PNAS RESEARCH ARTICLE | MEDICAL SCIENCES ENGINEERING OPEN ACCESS

Lipid nanoparticle GM-CSF replacement for autoimmune pulmonary alveolar proteinosis

Liming Lian[a,1], Bora Jang[a,1], Sebastian G. Huayamares[a,1], Avraham Shakked[a], Kara Gentry[a], Ryan Zenhausern[a], Afsane Radmand[b,c], Elisa Schrader Echeverri[a], Vaunita C. Parihar[d], Ricardo C. Guerrero-Ferreira[e], Randi Calkins[a], Daryll Vanover[a], Philip J. Santangelo[a], Hyejin Kim[a,2], and James E. Dahlman[a,2]

Affiliations are included on p. 9.

Edited by Gaurav Sahay, Oregon State University, Corvallis, OR; received May 12, 2025; accepted December 10, 2025 by Editorial Board Member Katherine A. Fitzgerald

Granulocyte–macrophage colony-stimulating factor (GM-CSF) deficiency drives autoimmune pulmonary alveolar proteinosis (aPAP), a disease characterized by impaired macrophage-mediated clearance of pulmonary surfactants. Clinical data suggest that inhaled recombinant GM-CSF reduces symptoms in aPAP patients, providing a rationale for mRNA-based GM-CSF replacement therapies. However, these require effective mRNA delivery after nebulization. Here, we report the iterative in vivo design of a lipid nanoparticle, named nebulized lung delivery 2 (NLD2), that efficiently delivers mRNA after nebulization. NLD2 carrying GM-CSF mRNA transfected alveolar macrophages in vivo, leading to interleukin-10 pathway activation and subsequent surfactant lipoprotein clearance. In a preclinical disease model of aPAP, GM-CSF mRNA delivery reduced surfactant protein thickness more than recombinant GM-CSF. These data support continued exploration of nebulized lipid nanoparticle therapies for aPAP.

LNP | nebulization | GM-CSF | autoimmune pulmonary alveolar proteinosis | mRNA

Significance

Autoimmune pulmonary alveolar proteinosis (aPAP) is a rare, life-threatening lung disease driven by granulocyte–macrophage colony-stimulating factor (GM-CSF) deficiency, which impairs alveolar macrophage-mediated surfactant clearance. While recombinant GM-CSF protein replacement confers some clinical benefit, messenger RNA (mRNA)-based replacement has been hindered by challenges in nebulized delivery. This study reports the development of a lipid nanoparticle, nebulized lung delivery 2 (NLD2), that overcomes the physical stress of nebulization to enable potent, cell-type-specific mRNA delivery to alveolar macrophages in vivo. In a preclinical aPAP model, nebulized NLD2 carrying GM-CSF mRNA outperformed recombinant GM-CSF in restoring macrophage function and surfactant clearance.

Autoimmune pulmonary alveolar proteinosis (aPAP) is often characterized by reduced granulocyte–macrophage colony-stimulating factor (GM-CSF) expression (1) and impaired macrophage functionality. Impaired macrophages are unable to clear pulmonary surfactants; the subsequent surfactant accumulation leads to dyspnea, hypoxemia, respiratory failure, and death (2–5). aPAP has been treated with whole lung lavage (6), but this is palliative and does not correct the cellular dysfunction that drives the disease. As a result, scientists have administered recombinant GM-CSF protein (rGM-CSF) to patients. Early clinical data suggest that rGM-CSF may improve alveolar macrophage function and surfactant homeostasis in patients (7, 8), supporting the exploration of targeted modalities to replace GM-CSF in the pulmonary epithelium.

One alternate approach to treat aPAP is to nebulize mRNA encoding GM-CSF. However, nebulized mRNA delivery is difficult because the process physically disrupts nanoparticles before they reach their target cells. Since this physical disruption is not experienced by nanoparticles given intravenously or intramuscularly, there are few structure–activity relationships scientists can use to design lipid nanoparticles (LNPs) that survive the nebulizer selection pressure. Relatedly, when scientists design LNPs for lung delivery, the difficulty and expense of in vivo nebulization studies make it difficult to test how numerous, chemically diverse LNPs behave in this context. Despite these challenges, labs have reported nebulized mRNA delivery in preclinical models using LNPs and cationic polymer-based nanoparticles (9–12). These contributions are important but have not yet led to positive data in patients; the most advanced LNP-mRNA drug nebulized in the clinic did not move beyond an initial phase 1/2 trial (13). We therefore focused on improving nebulized LNP delivery, identified a lead LNP named nebulized lung delivery 2 (NLD2), and used it to deliver mRNA encoding GM-CSF. We observed delivery in alveolar macrophages and the expected improvement in surfactant lipoprotein clearance. These data support further preclinical investigations of nanoparticle-mediated GM-CSF restoration for aPAP.

Results

NLD2 Can Be Concentrated and Delivers mRNA after Nebulization. We reported nebulized lung delivery 1 (NLD1), an LNP that delivered mRNA in murine lungs after nebulization (14). NLD1 was a four-component LNP that used a racemic 7C1 as its ionizable lipid. In subsequent studies, we found that ionizable lipid stereopurity can improve intravenous

Competing interest statement: J.E.D. advises Readout Capital.

This article is a PNAS Direct Submission. G.S. is a guest editor invited by the Editorial Board.

[1]L.L., B.J., and S.G.H. contributed equally to this work.

[2]To whom correspondence may be addressed. Email: hyejin.kim2@emory.edu or james.dahlman@emory.edu.

This article contains supporting information online at https://www.pnas.org/lookup/suppl/doi:10.1073/pnas.2511483123/-/DCSupplemental.

Published February 11, 2026.

LNP delivery (15, 16). To investigate whether stereopurity also improved nebulized LNP delivery, we formulated NLD1 to carry chemically modified mRNA encoding anchored nanoluciferase (AnLuc) using racemic 7C1 or stereopure 7C1. To isolate the effect of stereochemistry, both LNPs used the same four constituents as NLD1, were combined using the same molar ratios, and had the same lipid:mRNA mass ratio (10:1) (Fig. 1*A*). We nebulized both LNPs and administered them to mice at a dose of 20 μg. Two days later, we euthanized the mice, according to the approved procedure by the Institutional Animal Care and Use Committee of both the Georgia Institute of Technology and Emory University School of Medicine, performed a bronchoalveolar lavage (BAL), and quantified AnLuc bioluminescence in the lungs and BAL fluid (BALF). Consistent with the intravenous studies, bioluminescence was statistically higher in mice treated with the stereopure LNP (sNLD1) compared to mice treated with the racemic LNP (Fig. 1 *B* and *C*). Given that real-world nebulization requires stability at high concentrations, we then evaluated whether the sNLD1 withstood spin concentration. After increasing concentration by 2.5-fold using spinning, we observed particle degradation using dynamic light scattering (DLS) and cryo–electron microscopy (cryo-EM) (Fig. 1 *D* and *E*). To evaluate whether this lost structural integrity affected in vivo activity, we compared AnLuc bioluminescence after a 20 μg/mouse dose (without spin concentration) and 50 μg/mouse dose (with spin concentration). Bioluminescence decreased after spin concentration even though it was administered at a higher dose (Fig. 1*F* and *SI Appendix*, Fig. S1).

These data led us to design LNPs that retained i) structural integrity after concentration and ii) in vivo function after nebulization. After additional failed attempts to concentrate 7C1-based LNPs, we discarded this ionizable lipid. Instead, we synthesized three stereopure, biodegradable ionizable lipids named stereopure lipid 1, 2, and 3 (SL1, SL2, and SL3). To create a traditional, four-component LNP formulation, we mixed the ionizable lipids with DMG-PEG, the helper lipid 1,2-distearoyl-sn-glycero-3-phosphocholine (DSPC), and either cholesterol or budesonide

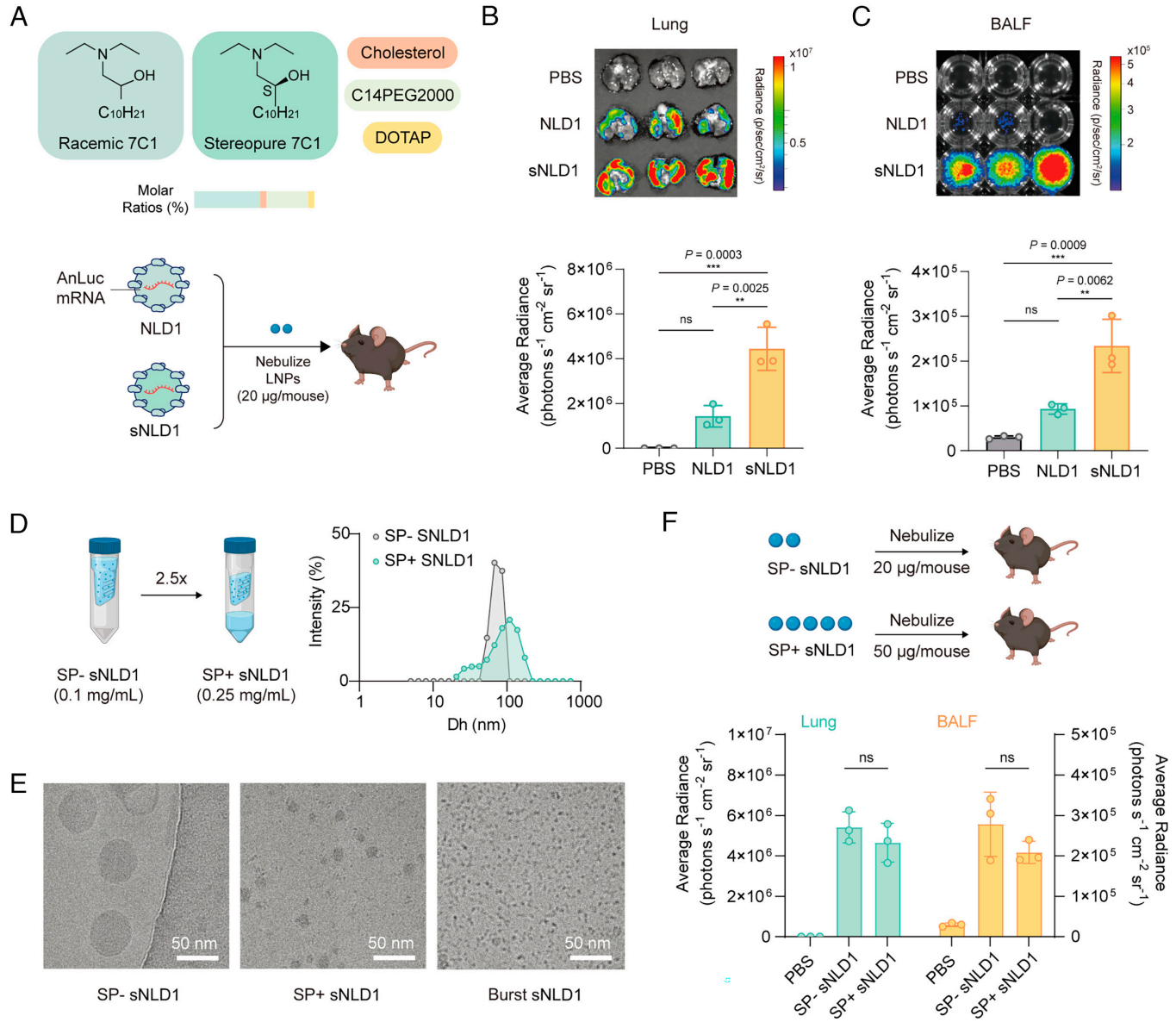

Fig. 1. sNLD1 enhanced lung delivery but was unstable during spin concentration. (*A*) sNLD1 was formulated with a stereopure form of the polymer–lipid 7C1. (*B* and *C*) Bioluminescence images and quantified AnLuc expression (*B*) in lungs and (*C*) in BALF on day two after NLD1 and sNLD1 nebulization as compared to PBS-nebulized mice. (*D*) DLS analysis for SP- and SP+ sNLD1. (*E*) cryo-EM images of sNLD1 with (SP+) or without (SP−) spin concentration and sNLD1 after Triton treatment (burst sNLD1). (*F*) Quantified AnLuc expression in lungs and BALF of SP− and SP+ sNLD1. Data are presented as mean ± SD (n = 3, biological replicates). "ns" stands for not significant ($P > 0.05$). $^{**}P < 0.01$, $^{***}P < 0.001$, analyzed by one-way ANOVA with Tukey's multiple comparisons test.

(Fig. 2*A* and *SI Appendix*, Fig. S2). We evaluated budesonide as a cholesterol substitute since its chemical structure is similar to cholesterol and it is FDA approved as an inhaled treatment for asthma (17). We found that the LNPs formulated with SL1, SL2, and SL3 all retained structural stability after fourfold concentration when measured by hydrodynamic diameter (Fig. 2*B*), polydispersity index (PDI) (Fig. 2*C*), and encapsulation efficiency (EE) (Fig. 2*D*).

We then compared the in vivo activity of the SL1-, SL2-, and SL3-based LNPs. After concentrating them fourfold, we administered them to mice at a dose of 80 μg/mouse. We made two observations. First, SL1-, SL2-, and SL3-based LNPs formulated with cholesterol led to higher AnLuc bioluminescence than the same LNPs formulated with budesonide. Second, LNPs made with SL2 maintained a stable morphology after concentration (Fig. 2*E*) and outperformed LNPs

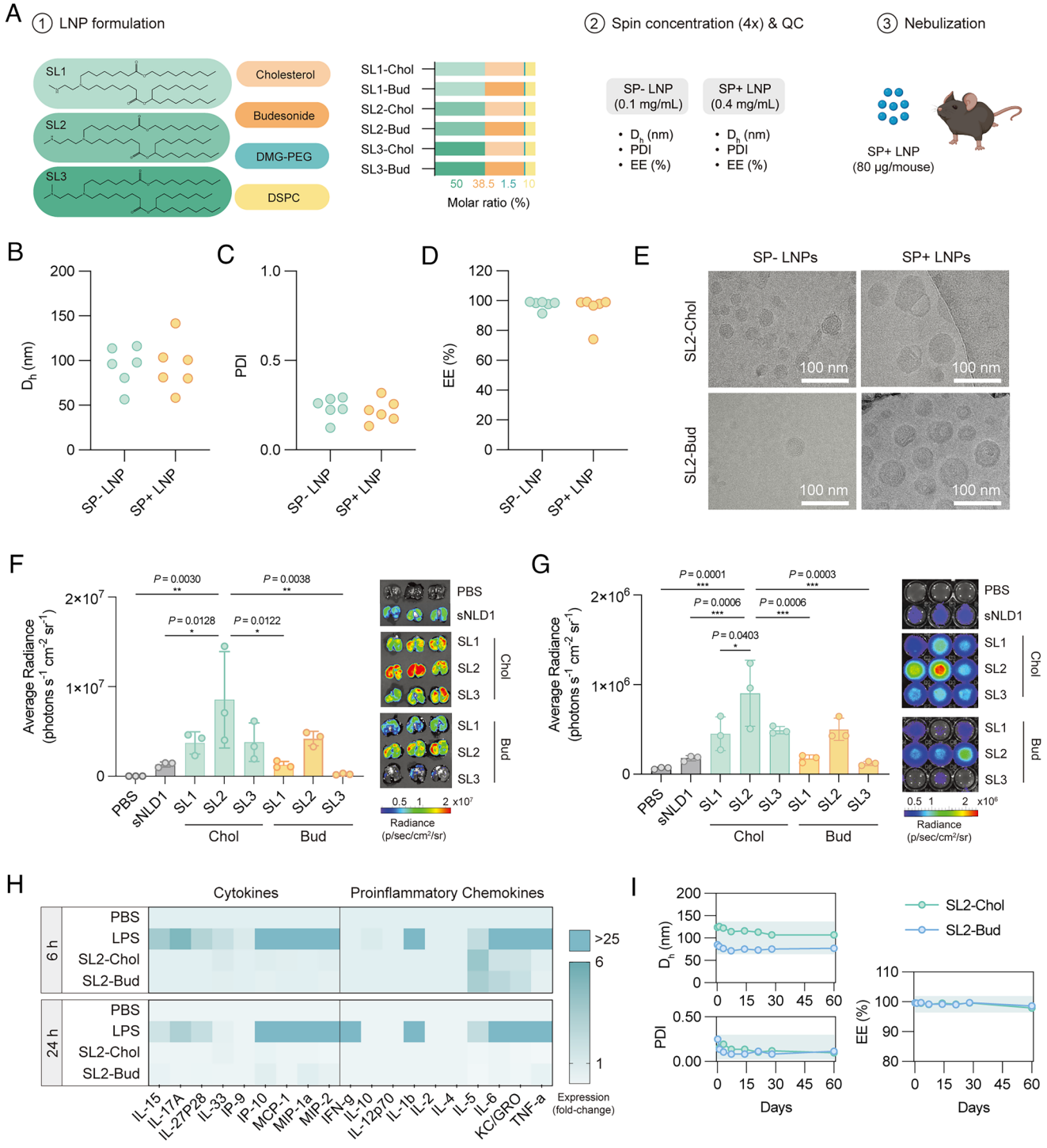

Fig. 2. LNP screening and characterization. (*A*) LNPs were formulated with stereopure and biodegradable lipid (SL1, SL2, or SL3), cholesterol or budesonide, DMG-PEG, and DSPC. Lipids were fourfold concentrated and nebulized to mice. (*B*) Hydrodynamic diameter (D_h), (*C*) PDI, and (*D*) EE of six individual LNPs before and after spin concentration. (*E*) Cryo-EM images of SL2-based LNPs. Bioluminescence images and quantified AnLuc expression (*F*) in lungs and (*G*) in BALF for six LNPs as compared to sNLD1 and PBS-nebulized mice. Data are presented as mean ± SD (N = 3, biological replicates). $*P < 0.05$, $**P < 0.01$, $***P < 0.001$, analyzed by one-way ANOVA with Tukey's multiple comparisons test. (*H*) BALF cytokine levels were analyzed from mice nebulized with PBS, SL2-Chol, SL2-Bud, or lipopolysaccharide (LPS) (1 mg kg^{-1}) at six and 24 h. Data represent mean fold changes relative to the PBS group (N = 3, biological replicates). (*I*), D_h, PDI, and EE changes of freeze–thawed SL2-Chol and SL2-Bud over 60 d.

formulated with SL1 and SL3 (Fig. 2 *F* and *G*). We coupled these in vivo delivery assays with toxicology and practical (e.g., freeze–thaw) studies (18). In mice that received 80 μg via nebulization, we evaluated 19 serum cytokines and proinflammatory chemokines six and 24 h after administration. We chose these timepoints since LNPs lead to inflammation at early timepoints (19). Both the cholesterol and budesonide LNPs formulated with SL2 led to interleukin-5 elevations at the 6-h timepoint in bronchoalveolar lavage fluid (BALF) and serum; this was resolved by the 24-h timepoint (Fig. 2*H* and *SI Appendix*, Fig. S3). We did not observe statistically significant elevations in the other 18 cytokines or chemokines. We also did not observe a statistically significant increase in neutrophils and monocytes in lung (*SI Appendix*, Fig. S4). We then evaluated stability after freeze–thawing the LNPs with 10% sucrose in PBS. Both SL2 LNPs exhibited consistent hydrodynamic diameter, PDI, and EE for 60 d (Fig. 2*I*). We also observed that freeze–thawed NLD2 LNPs showed no significant difference in luciferase expression compared to freshly prepared LNPs in lung tissue and BALF at 48 h after nebulization (*SI Appendix,* Fig. S5). Taken together, these concentration, delivery, toxicology, and freeze–thaw data led us to focus on the SL2-containing LNP formulated with cholesterol, which we named NLD2.

Nebulized lung delivery manuscripts often use whole-tissue luminescence as a readout for delivery. One limitation of these data is that they do not reveal which cell types are transfected. An ideal assay would i) generate unbiased readouts ii) in single cells iii) while preserving lung structure. To meet these criteria, we developed a bespoke, delivery-focused spatial transcriptomics approach. Specifically, we nebulized Ai14 mice with NLD2 and the budesonide-containing control LNP (NLD2-Bud) carrying Cre mRNA at a dose of 80 μg/mouse. In these mice, Cre protein excises a genomic stop preceding a tdTomato reporter. Thus, cells become tdTomato$^+$ if Cre mRNA is functionally delivered (i.e., turns into protein) into the cytoplasm (20). Five days after nebulization, we isolated the lungs, fixed them with paraformaldehyde (PFA), embedded them in paraffin, sectioned them, and analyzed them with spatial transcriptomics. To overlay delivery in these single, transcriptionally defined cells, we added a tdTomato mRNA pseudogene into the spatial transcriptomic workflow; since tdTomato mRNA is transcribed following Cre-mediated recombination, we were able to quantify functional mRNA delivery in the same single cells using tdTomato mRNA (Fig. 3*A*). Spatial transcriptomics divided lung cells into 15 subtypes: endothelial cells, alveolar type II cells, fibroblasts, ciliated cells, interstitial macrophages, lymphocytes, pericytes, vascular smooth muscle cells, alveolar macrophages, megakaryocytes, bronchiolar smooth muscle cells (SMCs), epithelial cells, lymphatic endothelial cells, adipocytes, and neutrophils (Fig. 3*B* and *SI Appendix*, Fig. S6). Consistent with our luciferase data, we observed higher tdTomato mRNA counts in mice treated with NLD2 than mice treated with NLD2-Bud or PBS (Fig. 3*B*). One key limitation of this approach is that it remains difficult to accurately quantify functional delivery. We anticipate that future efforts will address this concern, since a bespoke, delivery-focused spatial transcriptomics approach has the key advantage of preserving tissue structure. In this case, this allowed us to observe that NLD2 delivery occurred most often in alveolar regions near the airway and was particularly enriched in alveolar macrophages, which are a key cell type for aPAP.

NLD2-Mediated GM-CSF Delivery Improves Pulmonary Surfactant Clearance. GM-CSF knockout (GM-CSF$^{-/-}$) mice are an established preclinical model for aPAP (21) in part because they have reduced pulmonary surfactant clearance. We therefore evaluated whether NLD2 formulated to carry mRNA encoding GM-CSF could restore macrophage function in this model. As a control, we treated mice with rGM-CSF, which has led to encouraging results in clinical trials (7, 8). We administered either NLD2-GM-CSF (80 μg/mouse) or rGM-CSF (4 ng/mouse) (22) daily for 3 d, then isolated the lungs and BALF on day four. We then collected the lungs and imaged surfactant proteins A, B, C, and D with immunofluorescence; these surfactant proteins are cleared by functional alveolar macrophages (23, 24). Compared to PBS- and rGM-CSF-treated mice, NLD2 statistically reduced the thickness of all four surfactant proteins, suggesting that NLD2-GM-CSF treatment cleared surfactant proteins (Fig. 4 *A* and *B*). To complement these surfactant protein readouts, we used liquid chromatography–mass spectrometry to analyze the surfactant lipids in BALF after treatment. In the PBS-treated mice, lipidomic analysis identified 97 lipid species in the lung in ratios that were consistent with previous reports (*SI Appendix*, Fig. S7) (25, 26). Specifically, phosphatidylcholines (PC), phospholipids (PL), neutral lipids (NL), and sphingolipids (SL) constituted 80%, 10%, 5%, and 5% of the lipids, respectively (Fig. 4*C*). When we compared lipids in PBS and treated mice, we found that NLD2 treatment nonsignificantly reduced total lipid levels compared to PBS-treated mice, while rGM-CSF protein did not. We also found that the composition of the lipid subspecies changed (Fig. 4*D* and *SI Appendix*, Fig. S8). These data are early, and additional work will be required to understand whether changes in lipid subspecies are related to aPAP phenotypes.

Finally, when reading the aPAP clinical literature, we noted that the degree of both autoimmune-mediated macrophage dysfunction and disease severity varies significantly (27, 28) since some aPAP patients have nonzero GM-CSF activity. We therefore complemented the work in GM-CSF$^{-/-}$ mice with experiments in wild-type mice. Since these mice do not have dysfunctional lipid clearance and have normal pulmonary lipid thickness, we focused on evaluating the transcriptomic change in macrophages following GM-CSF treatment. We formulated NLD2 with GM-CSF mRNA and nebulized the LNP at 80 μg per mouse (*SI Appendix*, Fig. S9). One hour later we collected BALF cells, then quantified GM-CSF mRNA alongside the transcriptome in 32,797 transcriptionally defined single cells using single-cell RNA sequencing (scRNA-seq) (29). Unbiased clustering identified seven clusters: macrophages (CD68, cluster 1), T cells (CD3D, cluster 2), B cells (MS4A1, cluster 3), neutrophils (S100A9, cluster 4), epithelial cells (KRT18, cluster 5), dendritic (DC) cells (TRAF1, cluster 6), and natural killer (NK) cells (KLRD, cluster 7) (Fig. 4*E* and *SI Appendix*, Fig. S10) (30). When we quantified mouse GM-CSF (mGM-CSF) 1 h later, the percentage of cells that were GM-CSF$^+$ (Fig. 4*F*) and the mean expression of GM-CSF (Fig. 4*G*) increased significantly relative to baseline GM-CSF (i.e., the levels in wild-type mice treated with PBS). We found changes in macrophage signaling; specifically, when we evaluated macrophage subtypes using scRNA-seq (*SI Appendix*, Fig. S11), we found that macrophage subtype 2 increased from 1% of the macrophage population in PBS-treated mice to 26% of the macrophage population following NLD2-GM-CSF treatment (Fig. 4 *H* and *I*). We then used differential gene expression analysis to compare macrophage subtype 2 against the other macrophage subtypes (Fig. 4*J*), and analyzed the genes that were upregulated (over 1.5-fold) and significant ($P < 0.05$) using the unbiased pathway tool Reactome. We found that interleukin-10 (IL-10) signaling was the most upregulated pathway (Fig. 4*K*). IL-10 promotes macrophage polarization toward an anti-inflammatory phenotype, commonly referred to as M2 or alternatively activated macrophages (31), which promote the uptake and degradation of excess surfactant lipids and proteins through increased phagocytosis and lysosomal activity, restoring pulmonary homeostasis (32). These data suggest that GM-CSF replacement was sufficient to

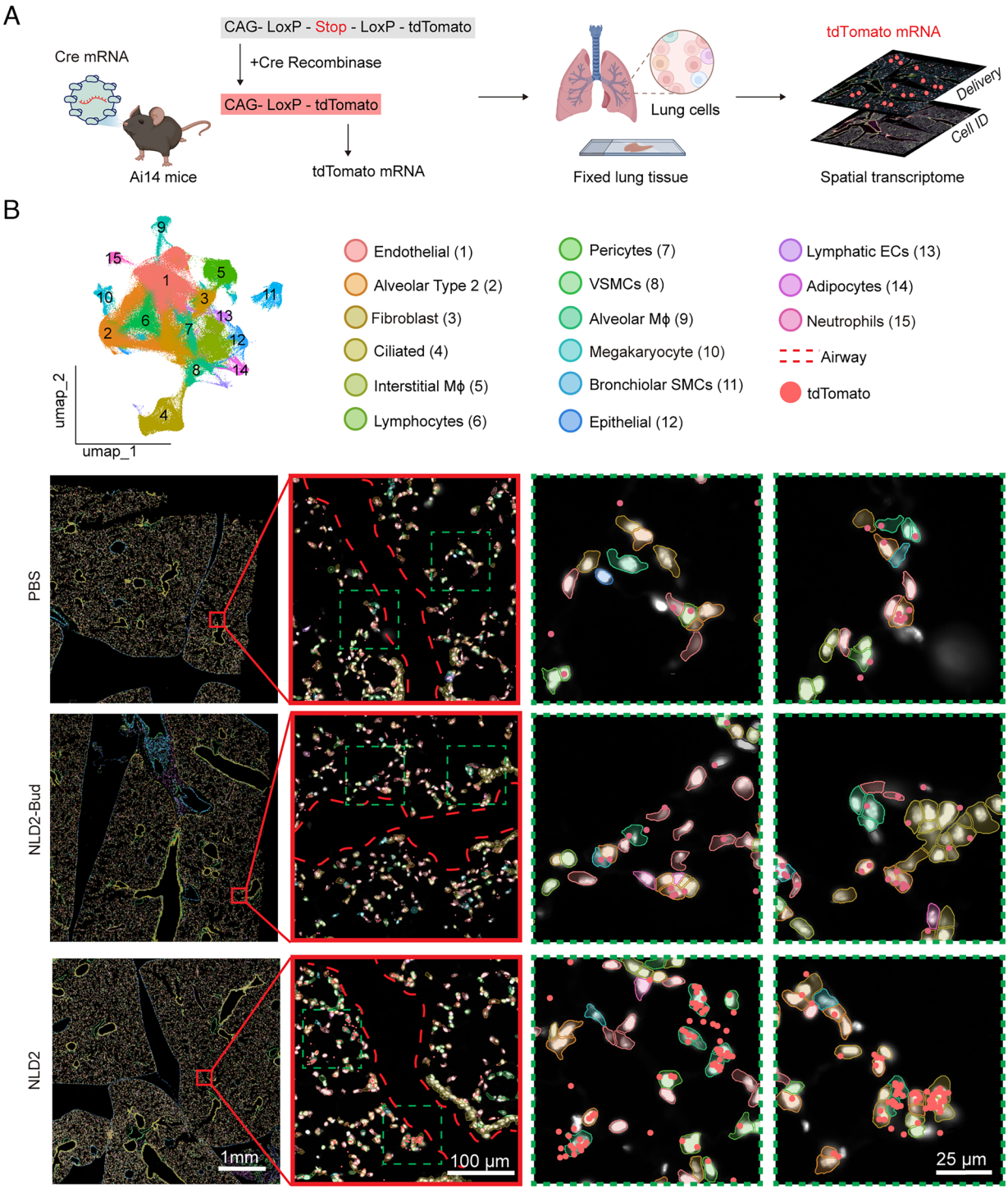

Fig. 3. Cell-type-specific NLD2 delivery. (*A*) Scheme of spatial transcriptomic workflow. Ai14 mice were nebulized with LNPs carrying Cre mRNA. Five days after nebulization, lungs were fixed and analyzed with spatial transcriptomics. (*B*) Cells of lungs treated with nebulized PBS, NLD2, or NLD2-Bud are divided into 15 subtypes by spatial transcriptomics. The first column of single-cell spatial imaging represents lung overview with highlighted region of interest (red square). The second column represents images with lung airway structure (red line) and a more specific highlighted region of interest (green square). The third and fourth columns represent different cell types and tdTomato expression (red) and are color coded according to the presented legend. The PBS sample does not show functional delivery (the few red spots are background and noise).

expand a subset of macrophages that are capable of clearing pulmonary surfactant lipids and proteins.

Discussion

VX-522, an inhaled LNP-mRNA developed by Vertex and Moderna, showed potential to restore CFTR function in the lungs of cystic fibrosis patients (33, 34). The FDA cleared the investigational new drug (IND) application in late 2022; however, Vertex later announced a pause in the multiple ascending dose segment of the phase 1/2 trial due to tolerability concerns (34, 35). A separate multiple ascending dose study, led by Arcturus Therapeutics, received IND clearance in 2024, dosed its patients starting in early 2025, and is ongoing without any clinical holds. Finally, Ethris announced phase 1 positive topline results in early 2025 with good tolerability (36, 37). Their subsequent advancement to phase 2a in mid-2025 has not resulted in a clinical

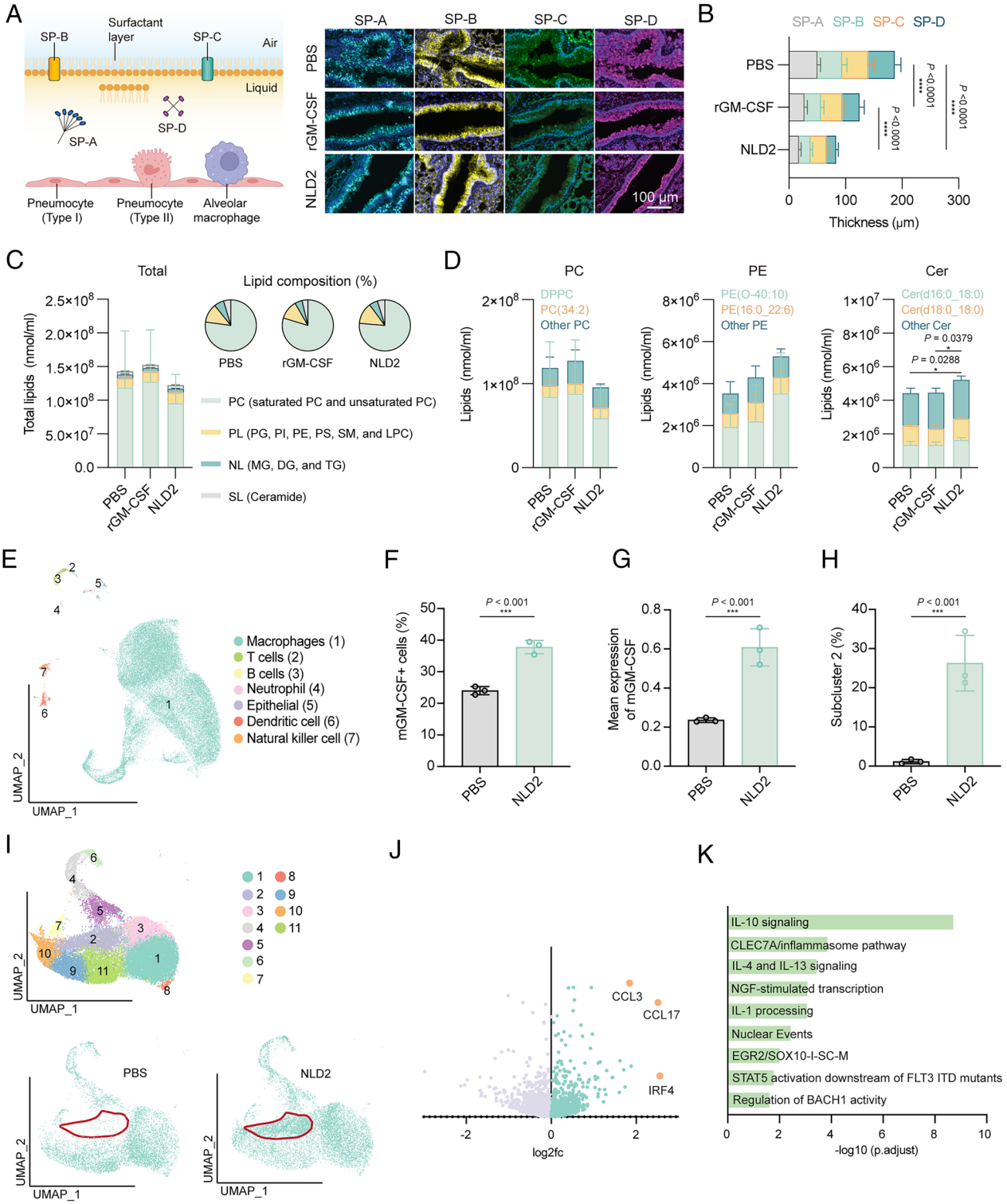

Fig. 4. NLD2-mediated GM-CSF mRNA delivery. Lung tissues and BALF of $(GM\text{-}CSF)^{-/-}$ mice were analyzed after rGM-CSF and NLD2-GM-CSF nebulization. (*A*) Immunofluorescence images of surfactant proteins (SP-A, SP-B, SP-C, and SP-D) in lung tissues (blue, nucleus; cyan, SP-A; yellow, SP-B; green, SP-C; magenta, SP-D). (*B*) Semiquantified thickness analysis of surfactant proteins. Data are presented as mean ± SD (N = 10, measured from 10 regions per sample). ***P < 0.001, analyzed by two-way ANOVA with Tukey's multiple comparisons test. (*C*) Total lipid count (*Left*) and relative compositional lipid analysis (*Right*) in BALF. The lipids were categorized into four lipid classes: PC (light green), PL (yellow), NL (green), and SL (gray). Furthermore, each lipid class was categorized with subclasses including saturated PC, unsaturated PC, phosphatidylglycerol (PG), phosphatidylinositol (PI), phosphatidylethanolamine (PE), phosphatidylserine (PS), sphingomyelin (SM), lysophosphatidylcholine (LPC), monoacylglycerol (MG), diacylglycerol (DG), and triacylglycerol (TG). (*D*) Composition changes of PC, PE, and Cer content in BALF. Data are presented as mean ± SD (N = 3, biological replicates). *P < 0.05, analyzed by two-way ANOVA with Tukey's multiple comparisons test. (*E*) BALF cells were categorized into seven clusters using UMAP: macrophages (cluster 1), T cells (cluster 2), B cells (cluster 3), neutrophils (cluster 4), epithelial cells (cluster 5), dendritic cells (cluster 6), and natural killer cells (cluster 7). Signature genes for each cluster facilitated cell-type identification. (*F*) The percentage of $mGM\text{-}CSF^{+}$ cells was higher in BALF cells transfected with NLD2. (*G*) Mean expression of mGM-CSF was overall higher in BALF cells transfected with NLD2 than in the PBS control. (*H* and *I*) Subclusters of macrophages and percentage of cluster 2 macrophages in whole macrophage population increased dramatically in the NLD2-transfected group. ***P < 0.001, analyzed by one-way ANOVA with Tukey's multiple comparisons test. (*J*) Differential gene expression analysis identified 6,484 genes uniquely regulated in cluster 2 macrophages compared to other macrophages. (*K*) Top 10 upregulated pathways in cluster 2 macrophages relative to other macrophages.

pause either. Taken together, these data suggest that improved LNP delivery remains an important need for nebulized mRNA therapies.

One further question is whether the addition of GM-CSF could drive toxicology. Although this question will require additional clinical data to answer, two lines of evidence support its evaluation. First, inhaled recombinant GM-CSF has been efficacious and safe in aPAP patients (38). Notably, the FDA issued a refuse-to-file letter to its manufacturer; however, this letter did not require additional clinical studies, instead citing manufacturing issues (39). Second, the disease is characterized in large part by the absence of GM-CSF; thus, there is a reasonable chance GM-CSF replacement would be tolerated.

Here, we provide evidence that LNP-mediated mRNA nebulization can affect macrophage signaling and influence surfactant clearance in mice. These data were generated with NLD2, an LNP that withstood both spin concentration and nebulization. Notably, our experience with NLD1 and its more effective stereopure version suggests that LNP compositions capable of surviving nebulization may not survive other physical processes such as spin-based concentration. We remain uncertain why the 7C1-based LNPs were able to withstand nebulization but not concentration, and we anticipate additional studies focused on the biophysical mechanisms driving these observations. Pragmatically, these data taught us to evaluate LNP structural integrity and in vivo functionality after spin concentration earlier in the LNP design process than we have previously.

NLD2 delivered mRNAs encoding two reporters: AnLuc and Cre. Although both are useful, we found Cre to be more informative, since it enabled us to evaluate delivery in transcriptionally defined single cells in situ using spatial transcriptomics. More specifically, the spatial data suggested that NLD2 transfected alveolar macrophages after nebulization; this gave us a rationale to focus on GM-CSF mRNA, since an ideal aPAP therapy would also preferentially transfect these cell types. The subsequent functional surfactant studies in GM-CSF$^{-/-}$ mice and signaling studies in wild-type mice were consistent with the spatial transcriptomics data, since in all cases, we observed evidence that macrophage activity changed as expected with GM-CSF restoration.

It is important to acknowledge the limitations of this paper. First, these studies were limited to mice, despite the fact that nonhuman primates are a better model of delivery in humans (15). We chose mice because there is no established model for aPAP in nonhuman primates. A related limitation is that although GM-CSF$^{-/-}$ mice are an established preclinical model for aPAP, it is unclear whether they recapitulate all the traits associated with the human disease. In addition, as with current nebulized mRNA therapies for primary ciliary dyskinesia and cystic fibrosis, we had to administer the drug regularly. Another limitation is that repeated long-term dosing might reduce drug efficacy over time. We are optimistic that next-generation mRNA (40, 41) with increased duration may lead to less frequent dosing. Also, future studies in more clinically relevant models (e.g., nonhuman primates) will provide more clinically relevant toxicology insight. Despite these limitations, this evidence supports additional preclinical studies evaluating nebulized LNP treatment of aPAP.

Materials and Methods

Lipid Synthesis. As shown in *SI Appendix*, Fig. S12, the branched heptadecane-9-ol (compound 1) was coupled with 8-bromooctanoic acid (compound 2) to form a bromo-substituted ester (compound 3), which then reacted with amine substrates to produce compound (compound 4) modified with different amine moieties. Compound 6 was obtained in the same way as compound 3, and the replacement of the terminal bromide with amine (compound 4) gave compound 7. The Boc groups in compounds 7a and 7b were deprotected to furnish compounds 8a and 8b.

mRNA Synthesis. GPI-anchored nanoluciferase (AnLuc) and Cre mRNA were prepared as described previously (42, 43). Synthetic DNA fragments encoding AnLuc and Cre were ordered as IDT DNA gBlocks. The sequences of the GPI anchor and nanoluciferase were previously reported (42). The gBlock was inserted into the PCR-amplified pMA7 vector with a threefold molar excess of the insert. Resulting IVT templates were purified by 0.8% agarose gel extraction and confirmed by Sanger sequencing. DNA templates were transcribed in vitro at 37 °C overnight using the HiScribe T7 kit (New England Biolabs) following the manufacturer's instructions. The transcription mixture was subsequently treated with DNase I to remove the DNA templates. After brief denaturation at 65 °C for 10 min, the transcripts were capped with the Cap1 structure and then enzymatically polyadenylated. For purity confirmation, the RNA products were analyzed by gel electrophoresis.

Nanoparticle Formulation. LNPs were formulated using a microfluidic system (NanoAssemblr Ignite, Precision Nanosystems) following established procedures. The mRNA and lipid phases were prepared separately in 10 mM citrate buffer and 100% ethanol, respectively. The two phases were microfluidically mixed at a flow rate ratio of 3:1 (mRNA phase:lipid phase). Resultant LNPs were diluted 40-fold in 10 mM Tris buffer (pH 7.4). The diluted LNPs were concentrated using 100-kDa Amicon Ultra centrifugal filter tubes (Sigma-Aldrich) at 1,000 × g for approximately 45 min until the desired concentration was reached. The concentrated LNPs were filtered through a 0.22 μm sterile sieve before nebulization.

LNP Characterization. The hydrodynamic diameters and PDI of LNPs were measured by DLS using a DynaPro Plate Reader III (Wyatt). EE was quantified with the Quant-iT™ RiboGreen™ RNA assay kit (Thermo Fisher Scientific). Briefly, LNPs (6 ng/μL) were mixed 1:1 with either 1× Tris-EDTA (TE; Thermo Fisher) or 2% Triton X-100 (Sigma-Aldrich) in 1× TE and incubated at 37 °C for 10 min. Afterward, a 1:100 dilution of RiboGreen reagent (Thermo Fisher) was added. Fluorescence intensity was measured using a PerkinElmer Victor X4 Microplate Reader (excitation 485 nm, emission 528 nm). Encapsulated mRNA concentration was calculated from standard curves.

Nebulization. A custom-built nose-only exposure system constructed using a clear PVC tee and animal restraints (CODA Small Mouse Holder, Kent Scientific) was used to hold the mice. A custom-designed nosecone, fabricated via 3D printing (3D Printing Tech) using flexible thermoplastic polyurethane, was used to connect the exposure setup. The nebulizer (Aeroneb, Kent Scientific) was attached to the upper inlet of a PVC tee, allowing aerosol delivery into the nose-only exposure chamber. Doses were introduced gradually into the nebulizer at a rate of 70 μL per droplet. After each droplet was nebulized, the clear PVC tee was inspected to ensure complete vaporization of the dose, which took approximately 15 to 45 s. Additional droplets were added until each animal received the intended dose. Mice were removed from the restraints after the vapor from the final droplet had fully dissipated.

IVIS Imaging. At 48 h post LNP administration, mice were euthanized, according to the approved procedure by the Institutional Animal Care and Use Committee of both the Georgia Institute of Technology and Emory University School of Medicine, and lung and BALF were collected for luminescence analysis. The samples were incubated in Nano-Glo luciferase substrate (Promega) diluted 1:50 in 1× PBS for 5 min. BALF samples were imaged directly in 96-well plates. Lung tissues were gently blotted to remove excess buffer and placed on black paper. Luminescence was measured using an IVIS imaging system (PerkinElmer) and quantified with Living Image software (PerkinElmer).

Freeze–Thawing of LNPs. Sucrose (NF, EP, JP, ChP, high purity, low endotoxin, Fisher Scientific) was dissolved in 1× PBS at 55% (w/v). LNPs in 10 mM Tris buffer were mixed with the sucrose solution at 10:2.2 (LNP:sucrose) ratio for a final sucrose concentration of 10% (w/v). LNPs were flash-frozen in liquid nitrogen and stored at ≤−80 °C until use. Hydrodynamic diameter, PDI, and EE were measured before and after freeze–thawing.

Characterization of LNPs by Cryo-TEM. For sample preparation, LNPs were applied onto 300-mesh copper grids coated with a perforated carbon film (1.2 μm holes spaced 1.3 μm apart; Quantifoil Micro Tools, Germany). Prior to

sample loading, the grids were glow discharged with a negative polarity for 15 s using a GloQube Plus glow discharge system (Quorum Tech, Laughton, UK). A 3 μL droplet of the sample was applied, blotted with filter paper for 1 s at room temperature and 100% humidity, and subsequently plunge-frozen into liquid ethane using a Vitrobot Mark IV (Thermo Fisher Scientific, Hillsboro, OR). The vitrified cryo-EM grids were stored in liquid nitrogen until imaging. For cryo-EM data acquisition, grids were transferred under liquid nitrogen temperatures using a Gatan 914 cryo-TEM sample holder and loaded into a JEOL JEM-2200FS TEM (JEOL, Japan) operating at 200 keV. Micrographs were recorded in low-dose mode with SerialEM software using a DE20 direct electron detector (Direct Electron, San Diego, CA) at nominal magnifications of 3 kx (overview images), 20 kx, or 80 kx, corresponding pixel sizes of 21.2, 2.9, and 0.8 Å per pixel, respectively.

Mouse Experiments. All animal experiments were conducted in accordance with protocols approved by the Institutional Animal Care and Use Committee of both the Georgia Institute of Technology and Emory University School of Medicine. Mice were maintained in the Georgia Institute of Technology or Emory University animal facilities. Wild-type C57BL/6J and GM-CSF$^{-/-}$ strains were obtained from The Jackson Laboratory.

Lung Lavage. BAL was performed using a customized catheter with a 25G needle (Becton Dickinson). After exposing the trachea through a small midline incision in the neck, a small puncture was made in the upper portion of the trachea, and the catheter was carefully inserted. The connection between the catheter and trachea was secured with surgical silk. One milliliter of warmed PBS (37 °C) was slowly injected into the lung through the catheter and then retrieved. The lavage process was repeated twice, and then the collected fluids were pooled for analysis.

Mouse Cytokine Analysis. BALF and blood samples were collected at 6 and 24 h following nebulized administration of PBS, NLD2-Bud, NLD2, or LPS (1 mg/kg, positive control). BALF samples were centrifuged at 500 × g for 5 min, and the supernatant was collected. Blood samples were allowed to clot at room temperature for 30 min before centrifugation at 2,000 × g for 15 min to isolate serum. Cytokine levels were detected using the Cytokine Panel 1 mouse kits and Proinflammatory Panel 1 mouse kits [Meso Scale Diagnostics (MSD) Assay Systems] according to the manufacturer's instructions. Plates were read and analyzed on the MESO QuickPlex SQ 120 (MSD).

Single-Cell Spatial Transcriptomics. Prior to tissue collection, the lung was perfused sequentially with ice-cold PBS and 4% PFA (PFA) (Electron Microscopy Sciences). After perfusion, a 1% agarose PBS solution (37 °C) was gently infused into the lung through the trachea using the catheter for BAL. The lung was then cooled on ice for 2 min before excision and immersion in 4% PFA for overnight fixation. Samples were sectioned, placed on Xenium slides (10× Genomics), and processed according to the manufacturer's protocol. Sections were subsequently counterstained with DAPI according to the 10× Genomics immunofluorescence procedure. Single-cell spatial data were analyzed and clustered using R and the Xenium Explorer software package.

GM-CSF mRNA Experiment. rGM-CSF (Bio-Techne) was dissolved in sterile PBS containing at least 0.1% human or bovine serum albumin. GM-CSF mRNA was synthesized by IVT and formulated with NLD2. The open reading frame (ORF) sequence of mouse GM-CSF was obtained from NCBI (GenBank: X03019.1). The GM-CSF gene was synthesized by Integrated DNA Technologies (IDT). The linear IVT template was generated by PCR amplification using forward and T120 extended reverse primers, followed by purification with the DNA Clean & Concentrator kit (Zymo Research). IVT was conducted using the MEGAscript™ T7 Transcription Kit (Invitrogen) at 37 °C for 2 h according to the manufacturer's instructions. During IVT, the mRNA was capped with Cap 1 (BOC Sciences), and all uridine residues were replaced with N1-methylpseudouridine-5′-triphosphates (N1-MeΨTPs, BOC Sciences). The IVT template was removed by DNase I treatment for 15 min at 37 °C. The final mRNA product was purified using lithium chloride precipitation and analyzed by gel electrophoresis to ensure purity and integrity. GM-CSF$^{-/-}$ mice were nebulized with PBS, rGM-CSF, or NLD2 for three consecutive days. On day four, BALF and lung tissues were collected for immunofluorescence staining and lipidomic analysis.

Immunofluorescence Staining. Lung tissues obtained after three consecutive days of treatment with PBS, rGM-CSF, or NLD2 were fixed with 4% PFA for 20 min and subsequently permeabilized with 0.1% Triton X-100 PBS solution for 15 min at room temperature. Samples were then blocked overnight at 4 °C with 1% BSA in PBS and co-incubated with the primary antibody solution at 4 °C overnight. After two washes with PBS, the samples were stained with the corresponding secondary antibodies. Finally, the samples were incubated with DAPI PBS solution at a ratio of 1:5,000 (v/v) for 15 min at room temperature. The images were acquired using an inverted fluorescence microscope and analyzed using QuPath software (v0.5.1).

Untargeted High-Resolution Lipidomics. BALF was collected after three consecutive days of treatment with PBS, rGM-CSF, or NLD2, and centrifuged at 500 × g for 5 min to remove debris. The supernatant was analyzed by high-resolution untargeted lipidomics using established liquid chromatography–tandem mass spectrometry (LC-MS/MS) protocols (44, 45). BALF samples were randomized, and lipids were isolated using an automated, high-throughput methyl tert-butyl ether (MtBE)-based method. In brief, 50 μL plasma was processed with methanol and internal standards to precipitate proteins, followed by MtBE-based lipid extraction, filtration, solvent removal, and reconstitution. A C18 column and a 15-min gradient were used with the Thermo Vanquish UHPLC system for samples analysis. Lipids were detected via a Thermo IDX Fusion mass spectrometer operated in both positive and negative ionization modes, with data-dependent acquisition for comprehensive untargeted profiling (46).

Single-Cell Multiomics Preparation. Beads provided by BD Rhapsody Single-Cell Analysis System were used for cell capture. Dead cells and red blood cells (RBCs) were removed using EasySep™ dead cell (Annexin V) and RBC (anti-TER119) removal kit (StemCell Technologies) following the manufacturer's instructions. The remaining cells were stained with a FITC-conjugated anti-mouse lineage antibody cocktail, and lineage negative cells were enriched using EasySep™ Release Mouse FITC Selection Kit (StemCell Technologies). Subsequently, oligo-tagged anti-mouse cell hashing antibodies (BioLegend) were added to uniquely label each sample. Following two PBS washes, the cell viability and numbers were determined and recorded for all samples. Cells were then pooled at equal ratios, and approximately 40,000 cells were loaded onto a BD Rhapsody cartridge for capture. cDNA libraries were prepared using the BD Rhapsody Whole Transcriptome Analysis Amplification Kit following the BD Rhapsody System mRNA Whole Transcriptome Analysis (WTA) and Sample Tag Library Preparation protocol (BD Biosciences). Final libraries were quantified using a Qubit Fluorometer and assessed with an Agilent Bioanalyzer prior to sequencing on an Illumina NovaSeq Plus platform (paired-end 150 bp; Novogene).

Processing of Sequencing Data. The data were processed using STARsolo (v2.7.9a) (47) with alignment to the GRCm39 mouse reference genome, counting only reads mapped to annotated exonic regions. All output files were loaded into Seurat (v4.0.4), and in summary, cells were log normalized to a scale factor of 10,000, then scaled using a linear transformation (48). Potential doublets were detected and filtered out using DoubletFinder (v3) (49). This was followed by PCA dimensional reduction and uniform manifold approximation and projection (UMAP)/t-SNE clustering. Cell clusters were annotated based on characteristic marker genes identified in mouse BALF cell populations. GM-CSF mRNA counts were imported into Seurat (v5.0.1) and were treated similarly to other multimodal datasets such as cellular indexing of transcriptomes and epitopes by sequencing (CITE-seq) (50). Further clustering and visualization were carried out in BBrowserX (51), where differential gene expression analyses were conducted within defined cell types. Functional pathway enrichment was assessed using the Reactome database 85 (52).

Statistics. A minimum of three biological replicates were analyzed for quantification, except for single-cell spatial transcriptomics (N = 1). All data are presented as the mean ± SD. Statistical analysis between groups was performed using GraphPad Prism (v.10.3.0). For experiments involving multiple conditions, statistical significance was determined by two-way ANOVA followed by Tukey's post hoc multiple-comparison test. The sample sizes (biological replicates), specific statistical tests, and main effects of our statistical analyses for each experiment are detailed in each figure legend. Differences were considered statistically significant at $P < 0.05$.

Data, Materials, and Software Availability. scRNA-seq raw data were deposited to the National Center for Biotechnology Information Sequence Read Archive database (SRX31915237 (53), SRX31915238 (54)) under project identifier PRJNA1412603 (55). The mouse genome GRCm39 can be accessed at NCBI (56). All other data are included in the article and/or *SI Appendix*.

ACKNOWLEDGMENTS. Figs. 1 *A*, *D*, and *F*, 2*A*, 3*A*, and 4*A* were created with BioRender. This research was funded by the NIH (U19AI171421, awarded to P.J.S. and J.E.D.)

Author affiliations: [a]Wallace H. Coulter Department of Biomedical Engineering, Emory University School of Medicine and Georgia Institute of Technology, Atlanta, GA 30322; [b]Petit Institute for Bioengineering and Biosciences, Georgia Institute of Technology, Atlanta, GA 30332; [c]Department of Chemical Engineering, Georgia Institute of Technology, Atlanta, GA 30332; [d]Cancer Tissue Pathology Shared Resource, Winship Cancer Institute, Emory University School of Medicine, Atlanta, GA 30322; and [e]Robert P. Apkarian Integrated Electron Microscopy Core, Emory University School of Medicine, Atlanta, GA 30322

Author contributions: L.L., B.J., S.G.H., P.J.S., H.K., and J.E.D. designed research; L.L., B.J., S.G.H., A.S., K.G., R.Z., A.R., E.S.E., V.C.P., R.C.G.-F., R.C., D.V., P.J.S., H.K., and J.E.D. performed research; L.L., B.J., S.G.H., A.S., K.G., R.Z., A.R., E.S.E., V.C.P., R.C.G.-F., R.C., D.V., P.J.S., H.K., and J.E.D. contributed new reagents/analytic tools; L.L., B.J., S.G.H., A.S., K.G., R.Z., A.R., E.S.E., V.C.P., R.C.G.-F., R.C., D.V., P.J.S., H.K., and J.E.D. analyzed data; and L.L., B.J., H.K., and J.E.D. wrote the paper.

1. N. Tanaka *et al.*, Lungs of patients with idiopathic pulmonary alveolar proteinosis express a factor which neutralizes granulocyte-macrophage colony stimulating factor. *FEBS Lett.* **442**, 246–250 (1999).
2. A. Kumar, B. Abdelmalak, Y. Inoue, D. A. Culver, Pulmonary alveolar proteinosis in adults: Pathophysiology and clinical approach. *Lancet Respir. Med.* **6**, 554–565 (2018).
3. B. C. Trapnell *et al.*, Pulmonary alveolar proteinosis. *Nat. Rev. Dis. Primers* **5**, 16 (2019).
4. B. C. Trapnell, J. A. Whitsett, Gm-CSF regulates pulmonary surfactant homeostasis and alveolar macrophage-mediated innate host defense. *Annu. Rev. Physiol.* **64**, 775–802 (2002).
5. T. L. Bonfield *et al.*, Peroxisome proliferator-activated receptor-gamma is deficient in alveolar macrophages from patients with alveolar proteinosis. *Am. J. Respir. Cell Mol. Biol.* **29**, 677–682 (2003).
6. I. Campo *et al.*, Whole lung lavage therapy for pulmonary alveolar proteinosis: A global survey of current practices and procedures. *Orphanet J. Rare Dis.* **11**, 115 (2016).
7. I. Campo *et al.*, Inhaled recombinant GM-CSF reduces the need for whole lung lavage and improves gas exchange in autoimmune pulmonary alveolar proteinosis patients. *Eur. Respir. J.* **63**, 2301233 (2024).
8. A. Ataya *et al.*, Pulmonary hypertension during high-dose GM-CSF therapy of autoimmune pulmonary alveolar proteinosis. *Pulm. Circ.* **14**, e70020 (2024).
9. S. Liu *et al.*, Charge-assisted stabilization of lipid nanoparticles enables inhaled mRNA delivery for mucosal vaccination. *Nat. Commun.* **15**, 9471 (2024).
10. A. Y. Jiang *et al.*, Combinatorial development of nebulized mRNA delivery formulations for the lungs. *Nat. Nanotechnol.* **19**, 364–375 (2024).
11. X. Bai *et al.*, Optimized inhaled LNP formulation for enhanced treatment of idiopathic pulmonary fibrosis via mRNA-mediated antibody therapy. *Nat. Commun.* **15**, 6844 (2024).
12. A. Suberi *et al.*, Polymer nanoparticles deliver mRNA to the lung for mucosal vaccination. *Sci. Transl. Med.* **15**, eabq0603 (2023).
13. S. G. Huayamares, R. Zenhausern, D. Loughrey, Nanocarriers for inhaled delivery of RNA therapeutics. *Curr. Res. Biotechnol.* **7**, 100200 (2024).
14. M. P. Lokugamage *et al.*, Optimization of lipid nanoparticles for the delivery of nebulized therapeutic mRNA to the lungs. *Nat. Biomed. Eng.* **5**, 1059–1068 (2021).
15. M. Z. C. Hatit *et al.*, Nanoparticle stereochemistry-dependent endocytic processing improves in vivo mRNA delivery. *Nat. Chem.* **15**, 508–515 (2023).
16. A. J. Da Silva Sanchez *et al.*, Substituting racemic ionizable lipids with stereopure ionizable lipids can increase mRNA delivery. *J. Control. Release.* **353**, 270–277 (2023).
17. A. Papi *et al.*, Albuterol–budesonide fixed-dose combination rescue inhaler for asthma. *N. Engl. J. Med.* **386**, 2071–2083 (2022).
18. B. Kim *et al.*, Optimization of storage conditions for lipid nanoparticle-formulated self-replicating RNA vaccines. *J. Control. Release* **353**, 241–253 (2023).
19. H. M. Nguyen *et al.*, mRNA-LNPs induce immune activation and cytokine release in human whole blood assays across diverse health conditions. *Mol. Ther.* **33**, 2872–2885 (2025).
20. C. D. Sago *et al.*, High-throughput in vivo screen of functional mRNA delivery identifies nanoparticles for endothelial cell gene editing. *Proc. Natl. Acad. Sci. U.S.A.* **115**, E9944–E9952 (2018).
21. B. B. Moore *et al.*, GM-CSF regulates bleomycin-induced pulmonary fibrosis via a prostaglandin-dependent mechanism. *J. Immunol.* **165**, 4032–4039 (2000).
22. J. A. Reed *et al.*, Aerosolized GM-CSF ameliorates pulmonary alveolar proteinosis in GM-CSF-deficient mice. *Am. J. Physiol. Lung Cell. Mol. Physiol.* **276**, L556–L563 (1999).
23. F. Brasch *et al.*, Surfactant proteins in pulmonary alveolar proteinosis in adults. *Eur. Respir. J.* **24**, 426–435 (2004).
24. T. Tschernig *et al.*, The importance of surfactant proteins–New aspects on macrophage phagocytosis. *Ann. Anat. Anat. Anz.* **208**, 142–145 (2016).
25. S. Karnati *et al.*, Quantitative lipidomic analysis of mouse lung during postnatal development by electrospray ionization tandem mass spectrometry. *PLoS One* **13**, e0203464 (2018).
26. E. Lee *et al.*, Alveolar macrophage lipid burden correlates with clinical improvement in patients with pulmonary alveolar proteinosis. *J. Lipid Res.* **65**, 100496 (2024).
27. X. Tian *et al.*, Inhaled granulocyte-macrophage colony stimulating factor for mild-to-moderate autoimmune pulmonary alveolar proteinosis–A six month phase II randomized study with 24 months of follow-up. *Orphanet J. Rare Dis.* **15**, 174 (2020).
28. G. Sheng *et al.*, Better approach for autoimmune pulmonary alveolar proteinosis treatment: Inhaled or subcutaneous granulocyte-macrophage colony-stimulating factor: A meta-analyses. *Respir. Res.* **19**, 163 (2018).
29. C. Dobrowolski *et al.*, Nanoparticle single-cell multiomic readouts reveal that cell heterogeneity influences lipid nanoparticle-mediated messenger RNA delivery. *Nat. Nanotechnol.* **17**, 871–879 (2022).
30. M. Liao *et al.*, Single-cell landscape of bronchoalveolar immune cells in patients with COVID-19. *Nat. Med.* **26**, 842–844 (2020).
31. R. L. Lopes, T. J. Borges, R. F. Zanin, C. Bonorino, IL-10 is required for polarization of macrophages to M2-like phenotype by mycobacterial DnaK (heat shock protein 70). *Cytokine* **85**, 123–129 (2016).
32. C. Malainou, S. M. Abdin, N. Lachmann, U. Matt, S. Herold, Alveolar macrophages in tissue homeostasis, inflammation, and infection: Evolving concepts of therapeutic targeting. *J. Clin. Invest.* **133**, e170501 (2023).
33. V. P. Incorporated, Vertex announces investigational new drug (IND) application for VX-522, mRNA therapy for people with cystic fibrosis, cleared by FDA (2022). https://investors.vrtx.com/news-releases/news-release-details/vertex-announces-investigational-new-drug-ind-application-vx-522.
34. ClinicalTrials.gov, A phase 1/2 study of VX-522 in participants with cystic fibrosis (CF) (2025). https://clinicaltrials.gov/study/NCT05668741.
35. V. P. Incorporated, Vertex reports first quarter 2025 financial results (2025). https://investors.vrtx.com/news-releases/news-release-details/vertex-reports-first-quarter-2025-financial-results.
36. Arcturus Therapeutics, Arcturus therapeutics receives clearance of an investigational new drug application to U.S. food and drug administration for ARCT-032, an investigational inhaled mRNA therapeutic to treat cystic fibrosis (2024). https://ir.arcturusrx.com/news-releases/news-release-details/arcturus-therapeutics-receives-clearance-investigational-new.
37. ClinicalTrials.gov, Safety, tolerability and efficacy study of ARCT-032 in people with cystic fibrosis (LunairCF) (2025). https://www.clinicaltrials.gov/study/NCT06747858.
38. B. C. Trapnell *et al.*, Phase 3 trial of inhaled molgramostim in autoimmune pulmonary alveolar proteinosis. *N. Engl. J. Med.* **393**, 764–773 (2025).
39. Savara Inc, Savara receives refusal to file (RTF) letter from the U.S. Food and Drug Administration (FDA) for the biologics license application (BLA) for MOLBREEVI* to treat patients with autoimmune pulmonary alveolar proteinosis (autoimmune PAP) (2025). https://investors.savarapharma.com/news/news-details/2025/Savara-Receives-Refusal-to-File-RTF-Letter-From-the-U-S--Food-and-Drug-Administration-FDA-for-the-Biologics-License-Application-BLA-for-MOLBREEVI-to-Treat-Patients-With-Autoimmune-Pulmonary-Alveolar-Proteinosis-autoimmune-PAP/default.aspx.
40. H. Chen *et al.*, Branched chemically modified poly(A) tails enhance the translation capacity of mRNA. *Nat. Biotechnol.* **43**, 194–203 (2025).
41. J. E. McGee *et al.*, Complete substitution with modified nucleotides in self-amplifying RNA suppresses the interferon response and increases potency. *Nat. Biotechnol.* **43**, 720–726 (2025).
42. K. E. Lindsay *et al.*, Aerosol delivery of synthetic mRNA to vaginal mucosa leads to durable expression of broadly neutralizing antibodies against HIV. *Mol. Ther.* **28**, 805–819 (2020).
43. P. M. Tiwari *et al.*, Engineered mRNA-expressed antibodies prevent respiratory syncytial virus infection. *Nat. Commun.* **9**, 3999 (2018).
44. D. I. Walker *et al.*, Metabolomic assessment of exposure to near-highway ultrafine particles. *J. Expo. Sci. Environ. Epidemiol.* **29**, 469–483 (2019).
45. D. I. Walker *et al.*, Metabolome-wide association study of anti-epileptic drug treatment during pregnancy. *Toxicol. Appl. Pharmacol.* **363**, 122–130 (2019).
46. H. E. Huneault *et al.*, Lipidome changes associated with a diet-induced reduction in hepatic fat among adolescent boys with metabolic dysfunction-associated steatotic liver disease. *Metabolites* **14**, 191 (2024).
47. K. Benjamin, Y. Dinar, D. Alexander, STARsolo: Accurate, fast and versatile mapping/quantification of single-cell and single-nucleus RNA-seq data. bioRxiv [Preprint] (2021). https://doi.org/10.1101/2021.05.05.442755 (Accessed 7 April 2025).
48. Y. Hao *et al.*, Integrated analysis of multimodal single-cell data. *Cell* **184**, 3573–3587.e3529 (2021).
49. C. S. McGinnis, L. M. Murrow, Z. J. Gartner, DoubletFinder: Doublet detection in single-cell RNA sequencing data using artificial nearest neighbors. *Cell Syst.* **8**, 329–337.e324 (2019).
50. M. Stoeckius *et al.*, Simultaneous epitope and transcriptome measurement in single cells. *Nat. Methods* **14**, 865–868 (2017).
51. L. Tri *et al.*, BBrowser: Making single-cell data easily accessible. bioRxiv [Preprint] (2020). https://doi.org/10.1101/2020.12.11.414136 (Accessed 3 March 2025).
52. J. Griss *et al.*, ReactomeGSA–Efficient multi-omics comparative pathway analysis. *Mol. Cell. Proteomics* **19**, 2115–2125 (2020).
53. L. Lian *et al.*, WT mouse BALF scRNA-seq gene expression library. NCBI SRA. https://www.ncbi.nlm.nih.gov/sra/SRX31915237[accn]. Deposited 23 January 2026.
54. L. Lian *et al.*, WT mouse BALF cell hashing library. NCBI SRA. https://www.ncbi.nlm.nih.gov/sra/SRX31915238[accn]. Deposited 23 January 2026.
55. L. Lian *et al.*, Lipid nanoparticle GM-CSF replacement for autoimmune pulmonary alveolar proteinosis. NCBI BioProject. https://www.ncbi.nlm.nih.gov/bioproject/?term=PRJNA1412603. Deposited 23 January 2026.
56. Genome Reference Consortium, Genome assembly GRCm39. NCBI. https://www.ncbi.nlm.nih.gov/datasets/genome/GCF_000001635.27/. Deposited 24 June 2020.